

Globular Cluster Scale Sizes in Giant Galaxies: Orbital Anisotropy and Tidally Under-filling Clusters in M87, NGC 1399, and NGC 5128

Jeremy J. Webb^{1,2} \star , Alison Sills¹, William E. Harris¹, Matías Gómez³,

Maurizio Paolillo^{4,5,6}, Kristin A. Woodley⁷, Thomas H. Puzia⁸

¹ *Department of Physics and Astronomy, McMaster University, Hamilton ON L8S 4M1, Canada*

² *Department of Astronomy, Indiana University, Bloomington IN 47405, USA*

³ *Departamento de Ciencias Físicas, Facultad de Ciencias Exactas, Universidad Andres Bello, Chile*

⁴ *Department of Physical Sciences, University of Napoli Federico II, via Cinthia 9, 80126 Napoli, Italy*

⁵ *INFN - Napoli Unit, Dept. of Physical Sciences, via Cinthia 9, 80126, Napoli, Italy*

⁶ *Agenzia Spaziale Italiana Science Data Center, Via del Politecnico snc, 00133, Roma, Italy*

⁷ *University of California, Santa Cruz, University of California Observatories, 1156 High Street, Santa Cruz, CA 95064, USA*

⁸ *Institute of Astrophysics, Pontificia Universidad Católica de Chile, Avenida Vicuña Mackenna 4860, Macul, 7820436, Santiago, Chile*

13 June 2021

ABSTRACT

We investigate the shallow increase in globular cluster half-light radii with projected galactocentric distance R_{gc} observed in the giant galaxies M87, NGC 1399, and NGC 5128. To model the trend in each galaxy, we explore the effects of orbital anisotropy and tidally under-filling clusters. While a strong degeneracy exists between the two parameters, we use kinematic studies to help constrain the distance R_β beyond which cluster orbits become anisotropic, as well as the distance $R_{f\alpha}$ beyond which clusters are tidally under-filling. For M87 we find $R_\beta > 27$ kpc and $20 < R_{f\alpha} < 40$ kpc and for NGC 1399 $R_\beta > 13$ kpc and $10 < R_{f\alpha} < 30$ kpc. The connection of $R_{f\alpha}$ with each galaxy’s mass profile indicates the relationship between size and R_{gc} may be imposed at formation, with only inner clusters being tidally affected. The best fitted models suggest the dynamical histories of brightest cluster galaxies yield similar present-day distributions of cluster properties. For NGC 5128, the central giant in a small galaxy group, we find $R_\beta > 5$ kpc and $R_{f\alpha} > 30$ kpc. While we cannot rule out a dependence on R_{gc} , NGC 5128 is well fitted by a tidally filling cluster population with an isotropic distribution of orbits, suggesting it may have formed via an initial fast accretion phase. Perturbations from the surrounding environment may also affect a galaxy’s orbital anisotropy profile, as outer clusters in M87 and NGC 1399 have primarily radial orbits while outer NGC 5128 clusters remain isotropic.

Key words: galaxies: kinematics and dynamics globular clusters: general

1 INTRODUCTION

The tidal field of a galaxy influences its globular cluster (GC) population by imposing a maximum size that each cluster can reach (e.g. von Hoerner 1957; King 1962; Innanen, Harris, & Webbink 1983; Jórdan et al. 2005; Binney & Tremaine 2008; Bertin & Varri 2008; Renaud et al. 2011). This maximum size is often referred to as the tidal radius r_t , the Jacobi radius, or the Roche lobe of the cluster. In all cases, it marks the distance from

the cluster at which a star will become unbound as it feels a stronger acceleration towards the host galaxy than it will towards the GC. von Hoerner (1957) predicted that:

$$r_t = r_{gc} \left(\frac{M}{2M_g} \right)^{1/3} \quad (1)$$

for a cluster of mass M on a circular orbit of radius r_{gc} , where M_g is the enclosed galactic mass.

Under the assumption that a galaxy can be approximated by an isothermal sphere ($M_g(r_{gc}) \propto r_{gc}$), we expect $r_t \propto r_{gc}^{2/3}$. Since there is no observational evidence that clus-

\star E-mail: webbjj@mcmaster.ca (JW)

ter central concentration c changes strongly with r_{gc} , the mean half-light radius r_h will follow the same scaling relation as r_t (Harris 1996; van den Bergh 2003). For the Milky Way, which gives us the only cluster population for which we have three dimensional positions and proper motions, we find $r_h \propto r_{gc}^{0.58 \pm 0.06}$ using positions and half-light radii from Harris 1996 (2010 Edition) and proper motions from Dinescu et al. (1999); Casetti-Dinescu et al. (2007, 2013). This is a mild but notable discrepancy from the nominal value of $\frac{2}{3}$.

Taking into consideration that only the projected galactocentric distance R_{gc} can be determined for GCs in other galaxies, the relationship between size and distance takes the form $r_t \propto R_{gc}^\alpha$, where $\alpha \sim 0.4-0.5$ for typical radial distributions (cluster density $\propto r_{gc}^{-2}$). However, observations in other galaxies appear to disagree with theoretical predictions. From a study of six giant elliptical galaxies, Harris (2009a) found the combined dataset was best fitted by an α of 0.11. This value is in agreement with observational studies of NGC 4594 ($\alpha = 0.19 \pm 0.03$ (Spitler et al. 2006; Harris et al. 2010)), NGC 4649 ($\alpha = 0.14 \pm 0.06$, (Strader et al. 2012)) M87 ($\alpha = 0.14 \pm 0.01$, (Webb et al. 2013b)), NGC 4278 ($\alpha = 0.19 \pm 0.02$, (Usher et al. 2013)) and NGC 1399 ($\alpha = 0.13 \pm 0.03$ (data from Puzia et al. (2014))). Looking at the metal poor (blue) and metal rich (red) cluster sub-populations in NGC 5128 separately, Gómez & Woodley (2007) found $\alpha = 0.05 \pm 0.05$ for the blue clusters and $\alpha = 0.26 \pm 0.06$ for the red clusters. Only the cluster population of the giant elliptical galaxy NGC 4365 in the Virgo cluster has a measured α of 0.49 ± 0.04 that is comparable to the expected range of 0.4-0.5 (Blom et al. 2012), which may indicate the galaxy has a different dynamical age or has undergone a different formation scenario than the galaxies listed above.

The discrepancy between Equation 1 and observed values of α may be attributed to assuming that all GCs have circular orbits in spherically symmetric isothermal tidal fields and that they fill their theoretical r_t . The first assumption is required in order for the tidal field experienced by the cluster to be static. However, galaxies will not necessarily have isothermal mass profiles or be spherically symmetric. A non-isothermal mass profile will alter the expected value of α , with a more strongly increasing cumulative mass with radius ($\frac{d(\log(M_g(r_{gc})))}{d(\log(r_{gc}))} > 1$) resulting in smaller values of α . Furthermore, no known GC has a truly circular orbit (Dinescu et al. 1999; Casetti-Dinescu et al. 2007, 2013). Eccentric orbits then subject the cluster to tidal heating and tidal shocks which can provide outer stars enough energy to escape the cluster and energize inner stars to larger orbits (e.g Küpper et al. 2010; Renaud et al. 2011; Webb et al. 2013a; Kennedy 2014). Clusters on eccentric orbits are also able to re-capture temporarily un-bound stars since the cluster's instantaneous r_t is also time-dependent. N -body models of GC evolution have shown that despite spending the majority of their lifetimes at apogalacticon, clusters with eccentric orbits lose mass at a faster rate (Baumgardt & Makino 2003) and appear smaller (Webb et al. 2013a) than clusters with circular orbits at apogalacticon. Hence incorporating the effects of orbital eccentricity on cluster evolution could reduce the discrepancy between theoretical and observed values of α . The situation will be complicated further if the cluster has

an inclined orbit in a non-spherically symmetric potential (Madrid et al. 2014; Webb et al. 2014) or if the cluster has been accreted by the host galaxy via a satellite merger such that its current orbit does not reflect the tidal field in which it formed and evolved (Miholics et al. 2014; Bianchini et al. 2015; Renaud & Gieles 2015; Miholics et al. 2015).

The second assumption, that all clusters fill their theoretical r_t , we now understand is also unrealistic. While a GC will naturally expand due to two-body interactions (Henon 1961), it is possible that certain clusters formed compact enough or expand slowly enough such that they have yet to reach the point of filling their r_t and effectively evolve in isolation. Observationally for such clusters, their limiting radius r_L (the radius at which the cluster's density falls to zero) is less than r_t . Observations of Galactic GCs have shown that only approximately $\frac{1}{3}$ of the population are tidally filling, in the sense that $r_L \sim r_t$ (Gieles et al. 2011). The remaining clusters in the Milky Way are still in the expansion phase and are considered to be tidally under-filling. Under-filling clusters have also been found in NGC 4649, where Strader et al. (2012) found no evidence for tidal truncation for clusters beyond 15 kpc and in NGC 1399, where Puzia et al. (2014) found no evidence for truncation beyond 10 kpc. Alexander & Gieles (2013) were able to reproduce the observed size distribution of Galactic GCs by assuming that all clusters form initially compact and then expand naturally via two-body interactions until they become tidally filling. After 12 Gyr of evolution, inner clusters which experience a strong tidal field and have small tidal radii have expanded to the point of being tidally filling. Outer clusters, with large tidal radii, still remain tidally under-filling after 12 Gyr since the outer tidal field is weak. Allowing clusters to become more under-filling with increasing r_{gc} offers a second explanation as to why observed values of α are noticeably less than theoretical predictions.

Understanding how the factors discussed above can influence α allows us to use the size distribution of GC populations to constrain many properties of their host galaxy, including its mass and orbital anisotropy profiles. In two previous studies of the giant elliptical galaxy M87 (Webb et al. 2012, 2013b), we explored the effects of orbital anisotropy and tidal filling on its GC population out to 110 kpc. We found that it was possible to reproduce the observed relationship between r_h and R_{gc} in M87 by allowing cluster orbits to be preferentially radial. However, the degree of radial anisotropy required to reproduce the size distribution of inner and outer region clusters was quite different. This discrepancy was partially minimized by allowing orbital anisotropy to change with r_{gc} , but the degree of radial anisotropy in the outer regions of M87 was still much higher than kinematic studies suggested (Côté et al. 2001; Strader et al. 2011). We were also able to match theory and observations by allowing all clusters to be under-filling, but we only explored the effects of clusters being under-filling by the same amount at all r_{gc} .

Given that clusters form with some initial size distribution and can be found over large ranges in R_{gc} , clusters can under-fill their r_t either because the local tidal field is weak or they formed extremely compact. The situation is complicated even further by the possibility that some clusters in a galaxy may be accreted. If a cluster that was tidally filling in its original host galaxy is accreted and ends up

with an orbit at a large R_{gc} , it can appear to be extremely under-filling. So instead orbital anisotropy and tidal filling are likely to be functions of r_{gc} (e.g. Côté et al. 2001; Prieto & Gnedin 2008; Zait, Hoffman, & Shlosman 2008; Weijmans et al. 2009; Gnedin & Prieto 2009; Ludlow et al. 2010; Kruijssen et al. 2012; Alexander & Gieles 2013). The next step is to then incorporate these two parameters into our model as functions of r_{gc} .

In this study, we consider the combined effects of orbital anisotropy and tidal filling on GC populations in the giant galaxies M87, NGC 5128, and NGC 1399. Since we are focused on giant elliptical galaxies which are spherically symmetric over the range of R_{gc} that our observational datasets cover, orbital inclination is not a contributing factor. It should be noted that some studies have found that M87 is not spherically symmetric at larger R_{gc} and that its surface brightness profile eventually reaches an ellipticity of 0.4 (e.g. Kormendy et al. 2009). Since this ellipticity is not high enough to significantly alter the behaviour of GCs in M87, we can still assume M87 is spherically symmetric in agreement with the many studies which have measured its mass profile (McLaughlin 1999; Strader et al. 2011; Agnello et al. 2014; Zhu et al. 2014). However, inclination will have to be considered in future studies if our approach is to be applied to non-spherically symmetric elliptical galaxies and disk galaxies. We also assume that all clusters in a given population have spent their entire lifetimes in the host galaxy. Miholics et al. (2014) showed that after a cluster is accreted by a host galaxy its size responds to its new potential within 1-2 GC relaxation times and evolves as if it has always orbited in the host galaxy. So while accreted clusters may maintain a kinematic signature of the accretion process, their *structural* parameters (which is the focus of this study) will reflect their *current* orbit in the host galaxy.

In Section 2 we introduce the three observational datasets used in our study and in Section 3 we re-introduce the theoretical model used to reproduce the observations. In Section 4 we first study how allowing the orbital anisotropy and tidal filling properties of clusters to change with r_{gc} affects the distribution of cluster sizes in each galaxy. We then explore the degeneracy between these two factors and make use of previous kinematic studies of each population to constrain our models even further. The best fit theoretical model for each galaxy is then discussed and the results of all three galaxies are compared in Section 5. We summarize our findings in Section 6.

2 OBSERVATIONS

In the following sections we summarize the datasets for M87, NGC 1399, and NGC 5128 used in this study. Table 1 lists the total number of GCs, radial range, and the measured value of α for each dataset. α is the slope of a log-log plot of median r_h versus R_{gc} , where the median r_h is calculated within radial bins containing 5% of the total cluster population. We also list the same properties when clusters are split into red and blue sub-populations. Red and blue clusters in M87 and NGC 1399 have very similar values of α , with the global M87 population having a slightly higher value of α overall. Red and blue clusters in NGC 5128 on the other hand have very different values of α , with the r_h of red clus-

Table 1. Properties of Observed Globular Cluster Populations

Galaxy	Population	N	Radial Range	α
M87	All	2335	0.1-108 kpc	0.13 ± 0.01
	Red	1211	0.1-106 kpc	0.10 ± 0.01
	Blue	1124	0.3-108 kpc	0.10 ± 0.01
NGC 1399	All	1266	2-49 kpc	0.09 ± 0.02
	Red	681	2-49 kpc	0.09 ± 0.02
	Blue	584	2-48 kpc	0.08 ± 0.02
NGC 5128	All	588	1.2-47 kpc	0.19 ± 0.03
	Red	310	1.2-43 kpc	0.29 ± 0.03
	Blue	278	1.4-47 kpc	0.03 ± 0.04

ters increasing steeply with R_{gc} compared to blue clusters. Overall, the increase in r_h with R_{gc} is much steeper in NGC 5128 than in M87 or NGC 1399.

While the colour and luminosity ranges of the M87 dataset are both thoroughly covered down to very low luminosity, in both NGC 1399 and NGC 5128 the data are incomplete for GCs much fainter than the luminosity function turnover. However, as we discuss in Sections 3.2 and 3.3, the incompleteness in mass range is factored into our model. The main parameter extracted from each dataset is the GC half-light radius, which is measured by fitting the surface brightness profile of each cluster with a King (1962) profile. For M87 (Webb et al. 2013b) and NGC 5128 (Gómez & Woodley 2007; Woodley et al. 2010b), surface brightness profile fits are done using the commonly used tool ISHAPE (Larsen 1999) and allowing the central concentration to be variable. For NGC 1399, GALFIT (Peng et al. 2010) is used to fit GC surface brightness profiles with King (1962) models (Puzia et al. 2014). r_h has been shown to be a robust parameter that can repeatedly be recovered using different surface brightness profile models (Webb et al. 2012) and different fitting routines (Webb et al. 2013a; Puzia et al. 2014) (including ISHAPE and GALFIT) when cluster sizes are comparable to the point spread function. Therefore using different fitting routines to measure cluster sizes in NGC 1399 will have a minimal affect on the results of this study, especially since our results only rely on the relative trends within each galaxy. Additionally, even though cluster sizes are measured in different wave bands, many studies have found that there are minimal differences when comparing sizes measured with different filters (e.g. Harris 2010; Strader et al. 2012; Webb et al. 2013b). And, since similar constraints are used to confirm GC candidates and minimize contaminants (magnitude, colour, quality of fit, and size), the observational datasets are as homogeneous as possible.

2.1 M87

M87 is a giant elliptical galaxy located at the centre of the Virgo cluster, with a distance modulus of $(m - M)_0 = 30.88$ (Pierce et al. 1994; Tonry et al. 2001). Hubble Space Telescope (*HST*) Advanced Camera for Surveys (ACS) / Wide Field Camera (WFC) images of the central 12 kpc of M87 in the F814W (*I*) and F606W (*V*) filters are taken from program GO-10543 (PI Baltz). The more recently completed

program GO-12532 (PI Harris) provided a combination of 8 ACS and WFC3 fields of view in the F814W and F475W filters of the outer regions of M87 ranging from 10 kpc to 110 kpc. See Webb et al. (2012) and Webb et al. (2013b) for a detailed description of how cluster candidates are selected and sizes are measured.

2.2 NGC 1399

NGC 1399 is a giant elliptical galaxy located at the centre of the Fornax cluster, with a distance modulus of $(m - M) = 31.52$ (Dunn & Jerjen 2006; Blakeslee et al. 2009). In this study we utilize archival *HST* images of NGC 1399 from program GO-10129 (PI Puzia). The 3×3 ACS mosaic in the F606W filter covers approximately $10' \times 10'$ out to a projected distance of approximately 50 kpc. A description of how cluster candidates are selected and how sizes are measured can be found in Puzia et al. (2014). It should be noted that while Puzia et al. (2014) introduced a cluster size correction function based on artificial cluster experiments, we use the uncorrected cluster sizes to keep the observational datasets in this study as homogeneous as possible. Hence the quoted value of α for NGC 1399 in Table 1 differs slightly from Puzia et al. (2014).

2.3 NGC 5128

NGC 5128 (Cen A) is a giant galaxy that is found in relative isolation, with a distance modulus of $(m - M) = 27.92$ (Harris 2010). We make use of Magellan/IMACS images of NGC 5128 to study its GC population out to a projected distance of approximately 40 kpc (Gómez & Woodley 2007). A description of how cluster candidates are selected and how sizes are measured can be found in both Gómez & Woodley (2007) and Woodley & Gómez (2010a).

3 MODEL

Our model (first introduced in Webb et al. (2012) and modified in Webb et al. (2013b)) generates a mock GC population that has the same distributions in projected distance, velocity and mass as the observed dataset. The model also has the capability to model sub-populations with different radial profiles and velocity dispersions separately, which we apply to the red and blue sub-populations in each galaxy. The central concentration distribution and mass to light ratios of model clusters are set equal to the Milky Way cluster population. Since our model has been modified to be applicable to any galaxy, we will re-introduce it here.

The projected radial distribution of clusters in each galaxy is obtained by fitting the observed number density profile ($n(R_{gc})$) with a modified two-dimensional Hubble profile:

$$n(R_{gc}) = \frac{n_0}{1.0 + (\frac{R_{gc}}{R_0})^2} \quad (2)$$

The red and blue radial distributions of GCs in M87 have previously been shown to follow a Hubble profile (Harris 2009b), and fitting Equation 2 to all three of our observed datasets yields reduced χ^2 (χ^2_ν) values of order

unity (see Sections 3.1 - 3.3 for the best fit values of n_0 and R_0 for red and blue clusters in each galaxy). Assuming the two-dimensional Hubble profile continues beyond the range of our observational datasets, Equation 2 is then transformed to obtain the three dimensional radial distribution from which cluster positions are randomly sampled (Binney & Tremaine 2008). Each model cluster is then assigned a three dimensional velocity based on the observed global line-of-sight velocity dispersion. Before assigning velocities, we first consider the anisotropy parameter (β), which is one of our two free parameters and controls the degree of orbital anisotropy within the GC system. β is defined as (Binney & Tremaine 2008):

$$\beta = 1 - \frac{\sigma_\theta^2 + \sigma_\phi^2}{2\sigma_r^2} \quad (3)$$

where σ_r , σ_θ , and σ_ϕ are the velocity dispersions for each spherical coordinate. In all cases, σ_θ and σ_ϕ are assumed to be equal. The isotropic case ($\beta = 0$) means that $\sigma_r = \sigma_\theta = \sigma_\phi$ are all equal to the line-of-sight velocity dispersion and velocities are randomly drawn from a Gaussian distribution. If β increases from zero then σ_r increases while σ_θ and σ_ϕ decrease such that the average of all three values still matches the observations and orbits become preferentially radial. The opposite occurs if β decreases from the isotropic case and orbits become preferentially circular.

We also allow for β to change as a function of r_{gc} . We assume the orbital anisotropy profile of a given galaxy is of the form:

$$\beta(r_{gc}) = \frac{1}{1 + (\frac{R_\beta}{r_{gc}})^2} \quad (4)$$

where the anisotropy radius R_β replaces β as one of the free parameters in our model. This form of $\beta(r_{gc})$ is in agreement with theoretical and observational studies which find that inner cluster orbits are primarily isotropic while orbits become preferentially radial with R_{gc} (e.g. Côté et al. 2001; Fall & Zhang 2001; Vesperini et al. 2003; Gnedin & Prieto 2009; Ludlow et al. 2010; Kruijssen et al. 2012). We also note that other functional forms of Equation 4 have been suggested in the literature, but studying the effects of different $\beta(r_{gc})$ profiles is beyond the scope of this study and will be addressed in the future.

Once a value of β has been given to each cluster, a mass is assigned based on the observed luminosity function of the dataset. The mass to light ratio of the model clusters is assumed to be equal to the mean value of $(\frac{M}{L})_V = 2$ found by McLaughlin & van der Marel (2005) for Milky Way GCs. The central concentration (c) of each cluster (log of the ratio between the cluster's core radius r_c to its limiting radius ($\log(\frac{r_c}{r_L})$)) is assigned based on the distribution of Milky Way GCs (Harris 1996), which is Gaussian with a mean of $c = 1.5$ and dispersion of 0.4.

Once each model cluster has been generated, the mass profile of the selected galaxy (see Figure 1 and Sections 3.1-3.3) is used to calculate the theoretical value of α that is expected assuming all clusters have circular orbits. Knowing the gravitational potential field also allows for the orbit of each individual cluster to be solved (Binney & Tremaine 2008). The resulting distribution of orbital eccentricities

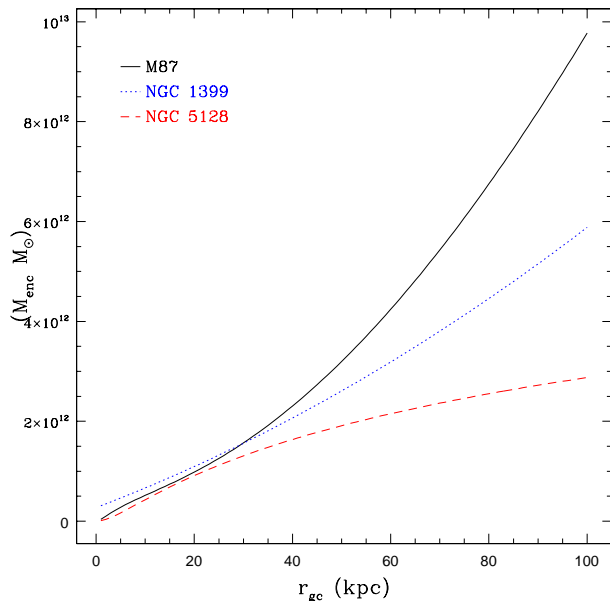


Figure 1. Total enclosed mass as a function of r_{gc} for M87 (black), NGC 1399 (blue), and NGC 5128 (red).

(and its dependence on r_{gc}) will then be dependent on β , the velocity dispersion of the GC population and the mass profile of the host galaxy. Hence two galaxies can have similar values of β but different distributions of cluster orbits.

Using the formalism of Bertin & Varri (2008), we next calculate each cluster's r_t at perigalacticon r_p . For clusters with eccentric orbits we use their orbital frequency Ω at r_p to calculate r_t as opposed to $\Omega = ((d\Phi_G(r)/dr)_{r_p}/r_p)^{1/2}$ which assumes the cluster has a circular orbit at r_p (Moreno et al. 2014). We then determine r_L at r_p based on our second free parameter $R_f = \frac{r_L}{r_t}$, also known as the tidal filling parameter. Hence R_f is a measure of how filling a cluster is at r_p , with clusters that fill only a fraction of their permitted r_t having $R_f < 1$.

We next assume that each model cluster can be represented by a King (1962) model, such that the limiting radius at r_p and the previously assigned central concentration set the cluster's surface brightness profile. However, R_f , r_L and r_h corresponding to the surface brightness profile are only valid when the cluster is located at r_p and will change as a function of orbital phase. Tidal heating, tidal shocks at r_p and the recapturing of temporarily unbound stars as a cluster moves away from r_p will cause r_h and r_L to increase as a function of orbital phase. We therefore correct the model r_h values for orbital eccentricity following Webb et al. (2013a) and Webb et al. (2013b), with r_h increasing by a maximum of 30% for highly eccentric clusters. No corrections are necessary for r_L and R_f since we do not compare these values to observations.

Similar to β , R_f can also be a function of a cluster's location in the tidal field. We specifically allow R_f to change as a function of r_{gc} via:

$$R_f(r_{gc}) = 1 - \frac{1}{1 + (\frac{R_{f\alpha}}{r_{gc}})^2} \quad (5)$$

where the filling radius $R_{f\alpha}$ becomes the free parameter. This form of R_f ensures clusters become less tidally filling as the tidal field becomes weaker (Alexander & Gieles 2013).

Finally, to best match the observed datasets, we apply magnitude and size cutoffs to the simulated dataset such that the model does not produce GCs that may exist but would not be observed. We also check to make sure the simulation does not produce any clusters with evaporation or infall times due to dynamical friction less than any observed clusters.

The individual input parameters and mass profiles of each galaxy are discussed in Sections 3.1 - 3.3. Since each galaxy has multiple estimations of various input parameters, we use the best available data that are also in line with the assumptions made by our model. Perhaps the most influential input parameter is our choice of mass profile. While a complete study of the effects that different mass profiles will have on our results is beyond the scope of our study, we note a different rate of increase in mass with r_{gc} will result in clusters having different values of r_t . More specifically a steeper increase in enclosed mass with r_{gc} will result in a shallower increase in r_t with r_{gc} . If the true values of r_t are smaller than the values calculated using the adopted mass profiles, then GCs must be more tidally filling and/or have a lesser degree of radial anisotropy. Hence our estimation of R_f will be a lower limit and our estimation of β will be a upper limit. The opposite will be true if the mass profile is shallower.

3.1 M87

The radial profile and luminosity function of our M87 dataset are listed in Table 2, along with the velocity dispersion parameters assigned to our theoretical cluster population. While observations of inner clusters sample the entire luminosity function, we incorporate into our model the fact that the luminosity function of outer clusters is only $\sim 50\%$ complete beyond the luminosity function turnover. In a kinematic study of the GC population of M87, Côté et al. (2001) found that blue clusters have a mean velocity (minus the galaxy's systemic velocity) of ~ 36 km/s with a dispersion of 412 km/s while red clusters have a mean velocity of 7 km/s and a dispersion of 385 km/s. They also suggested that the velocity dispersion may increase with R_{gc} . However more recent studies by Strader et al. (2011) and Zhu et al. (2014) found that the global velocity dispersion stays relatively constant with R_{gc} . Due to the larger datasets of Strader et al. (2011) and Zhu et al. (2014) and their more rigorous treatment of outliers, we will assume the velocity dispersion of M87 is constant at all r_{gc} . There is also no evidence in any of the galaxies presented in this study that either the mean velocity or velocity dispersion is dependent on cluster luminosity.

The galactic potential of M87 is taken directly from McLaughlin (1999) and has the form:

$$M_{total}(r) = M_{stars}(r) + M_{dark}(r) \quad (6)$$

$$M_{stars}(r) = 8.10 \times 10^{11} M_{\odot} \left[\frac{(r/5.1 \text{ kpc})}{(1 + r/5.1 \text{ kpc})} \right]^{1.67} \quad (7)$$

$$M_{\text{dark}}(r) = 7.06 \times 10^{14} M_{\odot} \times \left[\ln(1+r/560 \text{ kpc}) - \frac{(r/560 \text{ kpc})}{(1+r/560 \text{ kpc})} \right] \quad (8)$$

The stellar mass component (Equation 7) was determined by fitting model mass density profiles for spherical stellar systems (Dehnen 1993; Tremaine et al. 1994) to *B*-band photometry (de Vaucouleurs & Nieto 1978), assuming the stellar mass-to-light ratio of M87 is independent of radius. The dark matter component of M87 (Equation 8) was determined by combining X-ray observations of hot gas in the extended M87 halo, dwarf elliptical galaxies, and early-type Virgo galaxies to generate a Navarro-Frenk-White (NFW) dark matter halo (Navarro, Frenk & White 1997).

The overall mass profile is in general agreement with the more recent kinematic study of M87 performed by Strader et al. (2011), though the latter found evidence for a larger dark matter component within 20 kpc. Using the Strader et al. (2011) dataset, Agnello et al. (2014) also derived stellar and dark matter mass profiles for M87 by separating its cluster population into three sub-populations and noting their distinct radial distributions and velocity dispersions as a function of R_{gc} . The total mass of M87 as determined by Agnello et al. (2014) is comparable to McLaughlin (1999), although Agnello et al. (2014) found a more gradual increase in dark matter mass than McLaughlin (1999). Using an even larger GC dataset than Agnello et al. (2014) over a wider range of R_{gc} , Zhu et al. (2014) found a lower total mass within 100 kpc than McLaughlin (1999). However the gradient in the mass profiles of McLaughlin (1999) and Zhu et al. (2014), which is the key factor in setting how r_t increases with r_{gc} , are very similar out to an R_{gc} of 80 kpc. As noted by Strader et al. (2011), more extensive modelling of M87 and Virgo is required in order to better constrain its dark matter halo. Since the differences between the mass profiles discussed above are minimal (within the R_{gc} range of our observed dataset) and the McLaughlin (1999) model incorporates X-ray observations, we will utilize the mass profile as determined by McLaughlin (1999).

3.2 NGC 1399

The radial profile and luminosity function of our NGC 1399 dataset are listed in Table 3. Note that we have incorporated into our model that the luminosity function of our dataset is only complete to an absolute magnitude of -5.7. The velocity dispersion parameters assigned to our theoretical cluster population are taken from the most recent kinematic study of the NGC 1399 GC population, where Schuberth et al. (2010) found that blue clusters have a mean velocity of 11 km/s with a dispersion of 358 km/s and the red clusters have a mean velocity of 31 km/s with a dispersion of 256 km/s. While Schuberth et al. (2010) also suggested that the velocity dispersion of red and blue clusters may change with R_{gc} , we will assume these values remain constant with R_{gc} to stay consistent with our model for M87.

Schuberth et al. (2010) also derived a mass profile for NGC 1399 based on GC kinematics, although the authors assumed a value for the anisotropy parameter β . To stay consistent with the mass profile used for M87, we take the galactic potential of NGC 1399 as derived from *ROSAT* High Resolution Imager data by Paolillo et al. (2002). X-

Table 2. Simulated M87 Globular Cluster Population Input Parameters

Parameter	Value
Number of Clusters	
Blue	1124
Red	1211
Radial Distribution	Modified Hubble Profile
Blue Population	
σ_0	37.95 arcmin ⁻²
R_0	1.08'
Red Population	
σ_0	95.7 arcmin ⁻²
R_0	0.83'
Angular Distribution	Spherically Symmetric
Luminosity Function	Gaussian
$\langle M_V \rangle$	-7.6
σ_{M_V}	1.0
Velocity Dispersion	Côté et al. (2001)
Blue Population	
$\langle v \rangle$	-36 km/s
σ_v	412 km/s
Red Population	
$\langle v \rangle$	7 km/s
σ_v	385 km/s

ray emission from hot gas in NGC 1399 was used to make enclosed total mass (stars and dark matter) estimates at various distances. Since we require a functional form for the mass profile of each galaxy in order to solve the orbits and calculate the size of each model cluster, and since the data does not reflect a standard NFW profile, we fit the mass profile from Paolillo et al. (2002) with a quadratic function:

$$M_{\text{tot}}(r) = 2.74 \times 10^{11} M_{\odot} + 3.73 \times 10^{10} M_{\odot} \left(\frac{r}{1 \text{ kpc}} \right) + 1.87 \times 10^8 M_{\odot} \left(\frac{r}{1 \text{ kpc}} \right)^2 \quad (9)$$

3.3 NGC 5128

The radial profile and luminosity function of our NGC 5128 dataset are listed in Table 4. We have incorporated into our model the fact that our NGC 5128 cluster dataset is only 60% complete fainter than the luminosity function turnover. The velocity dispersion parameters assigned to our theoretical cluster population (also in Table 4) are taken from Woodley et al. (2010b). In a kinematic study of over 600 GCs, they determined that blue GCs have a mean velocity of 26 km/s with a dispersion of 149 km/s and red clusters have a mean velocity of 43 km/s with a dispersion of 156 km/s. Similar to NGC 1399, Woodley et al. (2010b) found evidence that the velocity dispersion of red and blue clusters changes with R_{gc} . However with no quantitative analysis of this radial variation, we again assume these values remain constant with R_{gc} . It is interesting to note that the velocity dispersions of the NGC 5128 cluster populations are approximately a factor of two smaller than in M87 and NGC 1399. This difference must have to do with M87 and NGC 1399 being massive galaxies located at the centres of a rich galaxy cluster while NGC 5128 is more or less in isolation. We will discuss the impact of environment further in Section 5.

Table 3. Simulated NGC 1399 Globular Cluster Population Input Parameters

Parameter	Value
Number of Clusters	
Blue	558
Red	668
Radial Distribution	Modified Hubble Profile
Blue Population	
σ_0	17 arcmin^{-2}
R_0	$1.1'$
Red Population	
σ_0	50 arcmin^{-2}
R_0	$0.8'$
Angular Distribution	Spherically Symmetric
Luminosity Function	Gaussian
$\langle M_V \rangle$	-7.3
σ_{M_V}	1.3
Velocity Dispersion	Schuberth et al. (2010)
Blue Population	
$\langle v \rangle$	11 km/s
σ_v	358 km/s
Red Population	
$\langle v \rangle$	31 km/s
σ_v	256 km/s

A mass profile of NGC 5128 that uses X-ray emission from hot gas currently does not exist. Instead we take the potential of NGC 5128 from enclosed total mass estimates from Woodley et al. (2010b) based on the kinematics of the NGC 5128 cluster population, which makes assumptions regarding the anisotropy profile of the cluster population. While we note that the mass profile of NGC 5128 has been determined via a different method than M87 and NGC 1399, it is in agreement with previous estimates taken from studies of HI gas shells (Schiminovich et al. 1994), planetary nebulae (Woodley et al. 2007; Peng et al. 2004) and other cluster datasets (Peng et al. 2004) and will still accurately reflect the true $M_{tot}(r)$. Fitting the total mass estimates with a NFW profile (Navarro, Frenk & White 1997), we find:

$$M_{tot}(r) = 1.74 \times 10^{14} M_{\odot} \times \left[\ln(1+r/8.2 \text{ kpc}) - \frac{(r/8.2 \text{ kpc})}{(1+r/8.2 \text{ kpc})} \right] \quad (10)$$

4 RESULTS

4.1 The Isotropic and Tidally Filling Case

We first compare our observed datasets to a baseline set of models in which the clusters are tidally filling with an isotropic distribution of orbits. To best compare to observations the three dimensional positions of our model clusters are projected onto a two-dimensional plane. In Figure 2 we have plotted the measured r_h of observed GCs (black) and theoretically determined r_h of model clusters (red) in all three galaxies. The solid lines show the median r_h as a function of R_{gc} .

Given the radial distribution of GCs and the mass profiles of M87 and NGC 1399, assuming each model cluster

Table 4. Simulated NGC 5128 Globular Cluster Population Input Parameters

Parameter	Value
Number of Clusters	
Blue	278
Red	310
Radial Distribution	Modified Hubble Profile
Blue Population	
σ_0	0.2 arcmin^{-2}
R_0	$3.7'$
Red Population	
σ_0	0.2 arcmin^{-2}
R_0	$4.0'$
Angular Distribution	Spherically Symmetric
Luminosity Function	Gaussian
$\langle M_V \rangle$	-8.0
σ_{M_V}	1.0
Velocity Dispersion	Woodley et al. (2010b)
Blue Population	
$\langle v \rangle$	26.0 km/s
σ_v	149.0 km/s
Red Population	
$\langle v \rangle$	43.0 km/s
σ_v	156.0 km/s

has a circular orbit at its current r_{gc} would yield values of α equal to 0.6. For NGC 5128, despite its shallower mass profile the radial distribution of GCs is such that $\alpha = 0.46$ (again assuming all clusters have circular orbits). Unfortunately, especially in the cases of M87 and NGC 1399, an isotropic distribution of orbits does not eliminate the difference between observed and theoretically predicted values of α . For M87 and NGC 1399, allowing clusters to have an isotropic distribution of orbits results in $\alpha = 0.55$. In the case of NGC 5128, the observations are surprisingly well matched by the isotropic case with $\alpha = 0.25$, with the model only slightly over-estimating cluster sizes at large R_{gc} . NGC 5128 is better fitted by the $\beta = 0$ and $R_f = 1$ model than M87 and NGC 1399 because its mass profile and smaller observed velocity dispersion results in clusters having a higher mean eccentricity and a smaller α . Since clusters are brought deeper into the potential well of the galaxy, they must also be more tidally filling (despite the galaxy being less massive) to match the higher global value of $\alpha = 0.19$ observed in NGC 5128.

Kinematic and structural studies of M87 and NGC 1399 do not support the idea of cluster populations being isotropic and tidally filling. Studies of galaxy formation and structure suggest that cluster orbits become preferentially radial and clusters become more tidally under-filling with increasing r_{gc} . As previously discussed in this study and in Webb et al. (2013a), α will be further decreased by allowing either the anisotropy parameter β to increase or the tidal filling parameter R_f to decrease. Increasing β serves to decrease cluster sizes as it results in cluster orbits being preferentially radial, bringing them deeper into the galactic potential of the galaxy. Decreasing R_f also results in clusters being compact and tidally under-filling, such that their observed size is less than r_t and they evolve as if they were in isolation. However, in Webb et al. (2013a) we only studied the effects of radi-

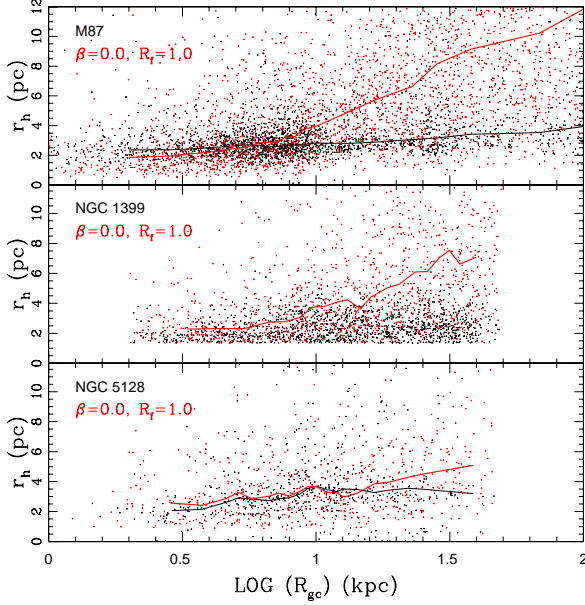


Figure 2. r_h vs $\log R_{gc}$ for observed globular clusters (black) and model clusters (red) in M87 (Top), NGC 1399 (Middle), and NGC 5128 (Bottom) assuming clusters have an isotropic distribution of orbits and are all tidally filling. The solid lines represent the median r_h calculated with radial bins containing 5% of the observed cluster population.

ally constant values of β and R_f on GC sizes. We explore the effects of these two parameters changing with r_{gc} in the following sub-sections.

4.2 The Effects of Orbital Anisotropy and Tidally under-filling Clusters

To explore the effects of radially dependent β and R_f , we re-run our simulations for $0 < R_\beta < 100$ kpc and $0 < R_{f\alpha} < 100$ kpc in search for the combination which provides the strongest agreement between our theoretical and observed cluster populations. We have initially assumed that red and blue clusters in each galaxy have the same orbital anisotropy and tidal filling profiles. To compare theory and observations, we determine the median r_h in 20 radial bins each containing 5% of the total population. A median half-light radius is also calculated for each mock GC population using the same radial bins as the observations. To measure how well a model reproduces the observed dataset, we calculate the χ^2_ν between the two median profiles via:

$$\chi^2_\nu = \frac{1}{N - n - 1} \sum_i^N \frac{(r_{h,obs}(R_{gc,i}) - r_{h,mod}(R_{gc,i}))^2}{r_{h,obs}(R_{gc,i}) + r_{h,mod}(R_{gc,i})} \quad (11)$$

where N is the total number of bins (20), n is the total number of fitted parameters (2), $r_{h,mod}(R_{gc,i})$ is the median half-light radius of the model in the i^{th} radial bin and $r_{h,obs}(R_{gc})$ is the median half-light radius of the observations in the i^{th} radial bin. The χ^2_ν value between our model and the observations is shown for the entire R_β and $R_{f\alpha}$ parameter space in Figure 3.

For M87 and NGC 1399, we see that high R_β - low

$R_{f\alpha}$ models can fit the observations just as well as low R_β - high $R_{f\alpha}$ models. The degeneracy is due to the previously mentioned fact that both parameters are used to decrease cluster sizes. In NGC 5128 the degeneracy is less clearly defined due to the smaller number of clusters and their significantly smaller observed velocity dispersion. A smaller velocity dispersion means that even moderate changes in R_β will not strongly affect the global kinematic properties of the model cluster population. With a lower number of clusters to sample the velocity dispersion with, the effect that changing R_β has on the model population is minimized further. Only very low values of R_β , such that the relative values of σ_r , σ_θ , and σ_ϕ differ dramatically, will the kinematic and structural properties of model clusters be noticeably altered. Hence any combination of moderate to large values of both R_β and $R_{f\alpha}$ yield a model population that is primarily isotropic and provides a match between theoretical and observed cluster sizes.

A second key issue that adds to the degeneracy between R_β and $R_{f\alpha}$ is the limited range in R_{gc} of our datasets. It is difficult to rule out higher values of R_β or $R_{f\alpha}$ based on cluster size alone since the majority of our observed clusters are found within 10 kpc of the galaxy centre. Hence high values of R_β or $R_{f\alpha}$ will not change the anisotropy or tidal filling profiles of inner region clusters, and only affect the outermost clusters in each galaxy. In order to remove some of the degenerate solutions in Figure 3 and identify acceptable values of R_β and $R_{f\alpha}$ we must therefore look beyond our own observational datasets and models.

4.3 Removing Degenerate Solutions

The degeneracy between R_β and $R_{f\alpha}$ in each galaxy indicates that there are multiple models which yield low values of χ^2_ν between the observed and theoretical median r_h profiles. To better constrain the parameter space, and eliminate some of the degeneracy between the two parameters, we can draw upon previous observational studies of each GC population. Kinematic studies of each galaxy have led to estimates of the global value of β , with some studies even suggesting possible anisotropy profiles. In order to eliminate some of our degenerate model solutions without placing undue weight on these previous studies, we only eliminate values of R_β that produce cluster populations with mean values of β that are outside the range of measured global values of β or outside the β range implied by an anisotropy profile. For a model consisting of N GCs, the mean β is simply $\langle \beta \rangle = \frac{\sum_{n=1}^N \beta(n)}{N}$ where $\beta(n)$ is the value of β at the given cluster's r_{gc} . $R_{f\alpha}$ on the other hand cannot as easily be constrained, as many issues including the initial size distribution of GCs, their tidal histories, and their merger/accretion histories can produce a range of different R_f profiles. Therefore we will focus on finding values of R_β that are also in agreement with kinematic studies of each galaxy.

4.3.1 M87

For M87, many kinematic studies exist that yield conflicting values of β and R_β . A study by Strader et al. (2011) inferred high global values of β (~ 0.4). Studies by Romanowsky & Kochanek (2001) and

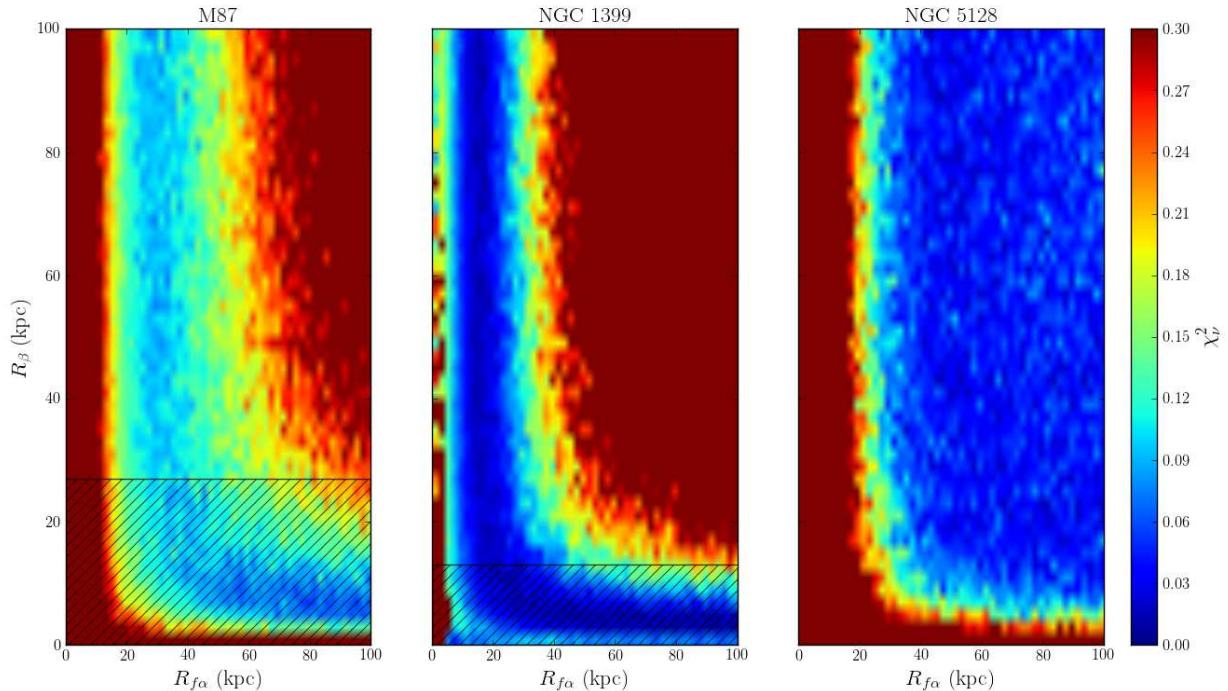


Figure 3. Degeneracy between R_β and $R_{f\alpha}$ for fits to the total cluster populations of M87 (left), NGC 1399 (middle) and NGC 5128 (right). Orbits go from preferentially radial to isotropic as R_β increases and clusters become preferentially tidally filling as $R_{f\alpha}$ increases. The colour scale corresponds to the χ^2_ν between our theoretical model and observations. Hatched out regions can be excluded based on kinematic studies of each galaxy (see Sections 4.4.1-4.4.3).

Murphy, Gebhardt & Adams (2011) on the other hand found that GCs in M87 are for the most part isotropic, with Murphy, Gebhardt & Adams (2011) inferring a small degree of radial anisotropy beyond 30 kpc. These three studies however go against the general findings of Deason et al. (2012), who in a study of 15 elliptical galaxies concluded that the distribution of cluster orbits in elliptical galaxies are primarily isotropic with a slight preference towards tangential orbits in some cases. This result was also found in M87 by Agnello et al. (2014). The most recent study regarding the kinematics of M87 by Zhu et al. (2014), which has the largest GC kinematic dataset to date out to 180 kpc, suggested that inner cluster orbits are tangentially biased ($\beta = -0.2$) with β increasing to 0.2 at 40 kpc and then decreasing back to 0 at 120 kpc. While the anisotropy profile suggested by Zhu et al. (2014) is in disagreement with Strader et al. (2011), it agrees with the results of Romanowsky & Kochanek (2001) and Murphy, Gebhardt & Adams (2011) while supporting the work of Deason et al. (2012) that the profiles might be partially tangentially biased. The fact that Zhu et al. (2014) found that β begins to decrease again at larger R_{gc} agrees with the general behaviour of β predicted by Agnello et al. (2014), but it does not support the idea that outer clusters have preferentially tangential orbits. Due to the large dataset and detailed method for determining the anisotropy profile of M87, we will use the results of Zhu et al. (2014) to remove degenerate model solutions that reproduce the distribution of cluster sizes in M87.

Based on the anisotropy profile suggested by Zhu et al. (2014), we exclude degenerate solutions where the mean β is greater than 0.2. Hence we can eliminate all models with R_β less than 27 kpc. Based on this constraint and our model fits to the distribution of cluster sizes in M87, it appears that $R_{f\alpha}$ must be between 25 and 40 kpc. The narrow acceptable range in $R_{f\alpha}$ suggests that $R_{f\alpha}$ might be the dominant parameter in determining the size profile of GCs in M87, with $R_{f\alpha}$ marking the distance where clusters transition from being tidally affected to being tidally unaffected. Having $R_{f\alpha}$ within this range results in the outermost clusters having R_f values between 0.06 and 0.14. Both of these values are comparable to the minimum R_f values in the Milky Way, which are approximately equal to 0.1. And since the outer clusters in M87 (many of which could have been tidally truncated before being accreted by M87) orbit in weaker tidal fields than the majority of Galactic GCs, we do not feel that $R_{f\alpha}$ can be constrained any further without additional r_h measurements of clusters beyond 40 kpc. To visualize the constraints that have now been placed on R_β and $R_{f\alpha}$, models that do not agree with the results of Zhu et al. (2014) have been hatched out in Figure 3.

4.3.2 NGC 1399

For NGC 1399, the degeneracy is larger than in M87 because the observational dataset contains almost half as many GCs and spans only $\frac{1}{3}$ the range in R_{gc} . Schuberth et al. (2010) modelled the cluster populations with β values between 0

and 0.5. Assuming the mean global β is less than 0.5, then R_β must be greater than 13 kpc. Similarly to M87, this constraint and our model fits to the distribution of cluster sizes allows us to set $R_{f\alpha}$ between 5 and 35 kpc. Since our NGC 1399 dataset only reaches out to 40 kpc, $R_{f\alpha}$ cannot be constrained any further and we can only conclude that the high R_β - low $R_{f\alpha}$ region (upper left of Figure 3) is acceptable. A detailed study of GC sizes in the outer regions of NGC 1399 will likely allow us to constrain R_f even further. For visualization purposes, models outside of the kinematically constrained range have been hatched out of Figure 3.

Comparing the acceptable ranges in $R_{f\alpha}$ for M87 and NGC 1399 indicates that $R_{f\alpha}$ is likely a reflection of tidal field strength. If we refer back to Figure 1, $M_g(r_{gc})$ increases at a slower rate in NGC 1399 resulting in r_t increasing at a faster rate compared to M87. If we assume the initial distribution of cluster sizes and their subsequent expansion is self-similar between galaxies, then the r_{gc} at which GCs are no longer tidally affected will be smaller in NGC 1399. Hence the allowed range in $R_{f\alpha}$ for NGC 1399 should centre around a smaller R_{gc} than M87, as observed. Furthermore, since the range in $R_{f\alpha}$ suggests that clusters in both galaxies become under-filling rather quickly, it is possible that the mild increase in r_h with R_{gc} observed in these galaxies is imprinted upon cluster formation. Hence only the innermost GCs and GCs with highly eccentric orbits will have their structural parameters altered by the tidal field of the galaxy.

4.3.3 NGC 5128

In a kinematic study of NGC 5128, Woodley et al. (2010b) also found that clusters could be approximated as having an isotropic distribution of orbits, with only a minor degree of radial anisotropy in the outermost regions (if at all). This is not surprising, since NGC 5128 was well fitted by an isotropic and tidally filling GC population in Section 4.1. Unfortunately, since no upper limit was placed on the global value of β we cannot constrain the parameter space beyond the χ^2_ν values presented in Figure 3. Hence we are forced to consider all models with R_β greater than 5 kpc and $R_{f\alpha}$ greater than 30 kpc. So while our model and kinematic studies support the conclusion that NGC 5128 is most likely isotropic and tidally-filling, we cannot rule out a slow increase in β or decrease in R_f with r_{gc} based on the kinematic and structural studies presented here.

4.4 The Orbital Anisotropy and Tidal Filling Profiles of M87, NGC 1399, and NGC 5128

We are now in a position to use our models to estimate the true values of R_β and $R_{f\alpha}$. The best fit models are illustrated for each galaxy in Figure 4. In all cases the χ^2_ν between the observed and theoretical median r_h profiles is less than unity. We also have plotted in Figure 5 the $\beta(r_{gc})$ and $R_f(r_{gc})$ profiles which correspond to each best fit model.

The allowed range of models for M87 has $R_\beta > 27$ kpc and $20 < R_{f\alpha} < 40$ kpc. NGC 1399 on the other hand has a wider range of acceptable models with $R_\beta > 13$ kpc and $10 < R_{f\alpha} < 30$ kpc. However within these ranges, the best fit models to M87 and NGC 1399 are very similar, with M87 having a $R_\beta = 60$ kpc and $R_{f\alpha} = 34$ kpc and NGC 1399 having $R_\beta = 76$ kpc and $R_{f\alpha} = 18$ kpc. So while cluster orbits

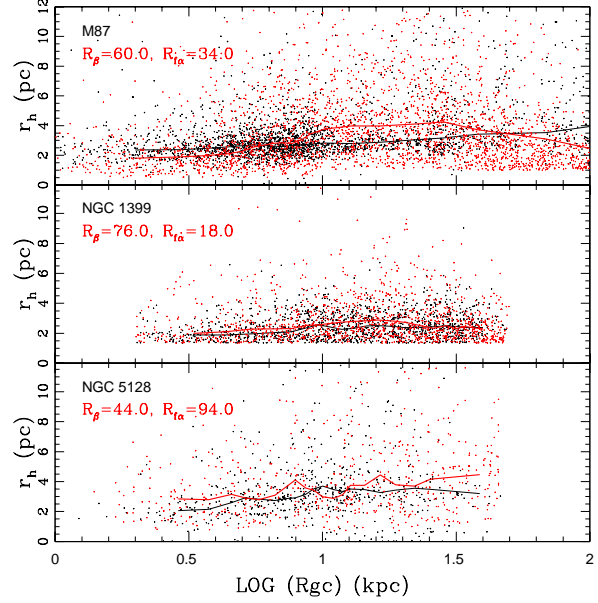


Figure 4. r_h vs $\log R_{gc}$ for observed globular clusters (black) and model clusters (red) in M87 (Top), NGC 1399 (Middle), and NGC 5128 (Bottom). Model clusters have anisotropy and tidal filling profiles as given by Equations 4 and 5, with the best fit values of R_β and $R_{f\alpha}$ indicated in each panel. The solid lines represent the median r_h calculated with radial bins containing 5% of the observed cluster population.

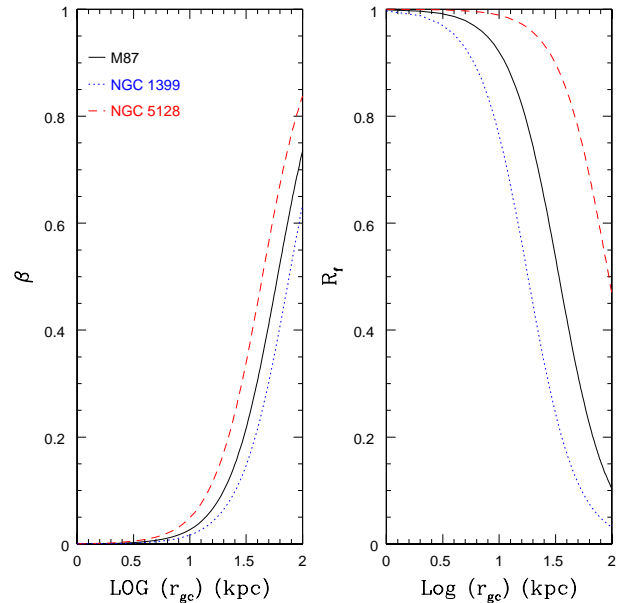


Figure 5. The anisotropy profile (left panel) and filling profile (right panel) that produce the theoretical distribution of cluster sizes that best matches the observed distributions in M87 (black), NGC 1399 (blue) and NGC 5128 (red).

become more radial with r_{gc} , it appears that the decrease in R_f is relatively steep, reaching values of 0.5 at 34 kpc and 18 kpc for M87 and NGC 1399 respectively. At the same time, the orbital anisotropy parameter β reaches 0.5 at approximately 60 kpc and 76 kpc in M87 and NGC 1399 respectively. Hence our models suggest NGC 1399 might be slightly more isotropic than M87, in agreement with Strader et al. (2011).

The accepted range of models for NGC 5128 is quite different from either M87 or NGC 1399, with $R_\beta > 5$ kpc and $R_{f\alpha} > 30$ kpc. The best fit model was $R_\beta = 44$ kpc and $R_{f\alpha} = 94$ kpc. However, as previously mentioned, the lower velocity dispersion and small number of clusters in NGC 5128 means that even with $R_\beta = 44$ kpc the model population is not significantly different from the $\beta = 0$ case. The high $R_{f\alpha}$ is required because the mean eccentricity is higher in NGC 5128 than the other two galaxies (given a mean $\beta \sim 0$) and clusters must be tidally filling to reproduce the higher observed α . It should be noted though that there is still a large degree of uncertainty associated with the best fit model to NGC 5128 due to the significant amount of degeneracy between R_β and $R_{f\alpha}$. In fact, we cannot clearly distinguish between the best fit model in Figure 5 and other model solutions that also accurately reproduce the distribution of cluster sizes. We even caution against introducing radial profiles in either β or R_f in the first place, since the χ^2_ν for the NGC 5128 model with $\beta = 0$ and $R_f = 1$ is only slightly improved compared to invoking β and R_f profiles.

Comparing Figure 4 to the isotropic and tidally filling cases (Figure 2), we see that for M87 and NGC 1399 we have significantly improved the discrepancy between theoretical and observed cluster sizes. However, in the case of M87, the discrepancy is still not completely removed. In M87, our model slightly underestimates cluster sizes within 10 kpc, over estimates cluster sizes between 10 and 50 kpc, and again underestimates cluster sizes in the outer regions. To achieve a better agreement between theoretical and observational sizes, we take a closer look in the next section at the properties of the red and blue sub-populations in each galaxy.

4.5 Separating the Metal Rich and Metal Poor Sub-Populations

In the previous section, we made the initial assumption that all clusters in a single galaxy share the same β and R_f profiles. However, it has long been known that GC populations in many types of galaxies can be divided into at least two sub-populations based on colour (e.g. Zepf & Ashman 1993; Larsen et al. 2001; Harris 2009b; Peng et al. 2006). Colour bimodality within cluster populations is often attributed to metallicity, with metal poor clusters being bluer than metal rich clusters (e.g. Zepf & Ashman 1993; Brodie & Strader 2006). Since this bimodality is observed over a wide range of galaxy masses and types (Harris et al. 2015), it is believed that the production of a two (or more) component GC population is an important step inherent to all galaxy formation and evolution mechanisms.

Observational studies have identified many structural and kinematic differences between these two sub-populations. A common observation within GC populations (including the populations presented here) is

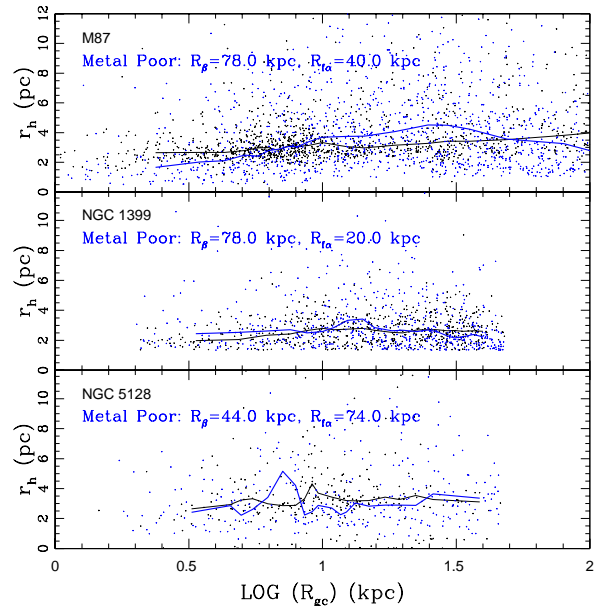


Figure 6. r_h vs $\log R_{gc}$ for observed metal poor globular clusters (black) and model clusters (blue) in M87 (Top), NGC 1399 (Middle), and NGC 5128 (Bottom). Model clusters have anisotropy and tidal filling profiles as given by Equations 4 and 5, with the best fit values of R_β and $R_{f\alpha}$ indicated in each panel. The solid lines represent the median r_h calculated with radial bins containing 5% of the observed cluster population.

that red GCs have half-light radii that are on average 20% (~ 0.4 pc) smaller than blue GCs (e.g. Kundu & Whitmore 1998; Kundu et al. 1999; Larsen et al. 2001; J rdan et al. 2005; Harris 2009a; Harris et al. 2010; Paolillo et al. 2011; Blom et al. 2012; Strader et al. 2012; Woodley 2012; Usher et al. 2013). The size difference is likely due to the red and blue sub-populations having different formation, dynamical and stellar evolution histories (e.g. Kundu & Whitmore 1998; J rdan 2004; J rdan et al. 2005; Harris 2009a; Sippel et al. 2012; Schulman et al. 2012). As discussed in Section 4.3, kinematic studies of GC populations find that red and blue sub-populations have noticeably different radial profiles and velocity dispersions, with some studies even suggesting that red and blue clusters have different β profiles as well (e.g. C t  et al. 2001; Schuberth et al. 2010). Therefore, we have elected to repeat the fitting process, but with the red and blue clusters modelled separately. The final comparison between our models and observations is illustrated in Figure 6 for metal poor clusters and Figure 7 for metal rich clusters.

By modelling metal poor and metal rich clusters separately we slightly improve the χ^2_ν between the observed and theoretical median r_h profiles of M87 and NGC 1399, with all χ^2_ν values again being less than 1. For M87, our model suggests that red clusters have a smaller R_β (more radial orbits) than blue clusters. Our study also finds that red clusters become tidally under-filling very quickly with r_{gc} compared to blue clusters. The different R_f profiles are in agreement with observational studies that found red clusters are on average smaller than blue clusters at all R_{gc} . For NGC 1399, the best fit anisotropy profiles to red and

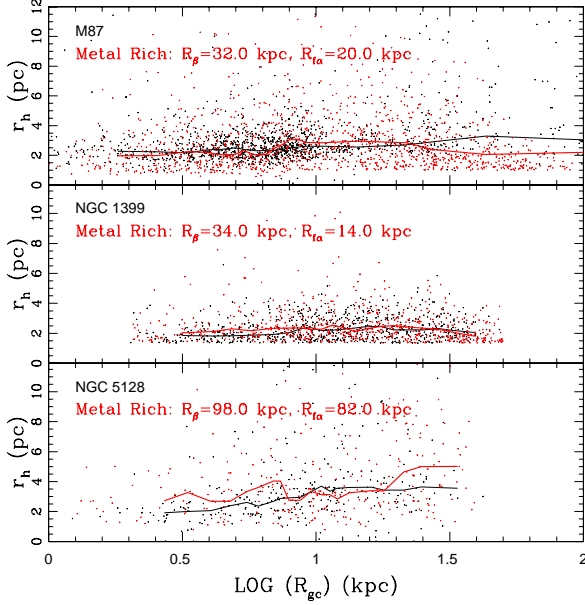


Figure 7. r_h vs $\log R_{gc}$ for observed metal rich globular clusters (black) and model clusters (red) in M87 (Top), NGC 1399 (Middle), and NGC 5128 (Bottom). Model clusters have anisotropy and tidal filling profiles as given by Equations 4 and 5, with the best fit values of R_β and $R_{f\alpha}$ indicated in each panel. The solid lines represent the median r_h calculated with radial bins containing 5% of the observed cluster population.

blue clusters are almost identical to M87. Also similar to M87, red clusters in NGC 1399 have lower values of R_β and $R_{f\alpha}$ than blue clusters. The only difference between the two galaxies is that clusters in NGC 1399 become under-filling slightly quicker than M87, which is likely a result of the tidal field in NGC 1399 being weaker than in M87 since it is less massive.

In NGC 5128, allowing red and blue clusters to have different values of R_β and $R_{f\alpha}$ yields much higher χ^2_ν values than either the isotropic and tidally filling case or when the sub-populations were given the same R_β and $R_{f\alpha}$ values. While this observation may be a result of the previously discussed issues regarding the degeneracy between R_β and $R_{f\alpha}$ in NGC 5128, it appears the galaxy is still best described as a singular tidally filling population with a mostly isotropic distribution of orbits.

5 DISCUSSION

Our model reproduces a realistic GC system by allowing cluster orbits to become more radial with r_{gc} , letting clusters become less tidally filling with r_{gc} and includes the possibility of modelling the red and blue cluster sub-populations separately. After applying the model to M87, NGC 1399, and NGC 5128 we can now discuss the best fit profiles to each galaxy in further detail.

5.1 M87

The lowest χ^2_ν between our model and observed GCs occurred when red and blue clusters were modelled independently. The fact that the best fit model for red and blue clusters implies the population becomes radially anisotropic with r_{gc} is in agreement with the idea that giant galaxies form through the hierarchical merging of dwarf galaxies that combine to form a central massive galaxy (Kravtsov & Gnedin 2005; Tonini 2013; Li & Gnedin 2014; Kruijssen 2014). While some clusters will form early in the small halos which make up the host galaxy, most of the GC population in a giant galaxy has been added via the accretion of dwarf galaxies. With ? finding that massive galaxies with a large population of accreted stars will have a high degree of radial anisotropy at large r_{gc} , a similar result can be expected for outer GCs in massive galaxies. The identification of shells, arcs, and streams of kinematically distinct GCs in M87 suggests that the outer regions of M87 have been built up via a continuous infall of material that is still ongoing today (Strader et al. 2011; Romanowsky et al. 2012; D’Abrusco et al. 2013, 2014a,b, 2015; Longobardi et al. 2015). Strader et al. (2011) and Romanowsky et al. (2012) also suggested that clusters beyond 40 kpc are being dynamically perturbed by nearby galaxies. Continuous perturbations could also result in many of the outer clusters being energized to eccentric orbits and further increase the degree of radial anisotropy in the outer regions of brightest cluster galaxies (BCGs).

Models of giant galaxies that form via the accretion of smaller galaxies also found the majority of clusters which form in the central host are metal-rich while the majority of accreted clusters are metal poor, suggesting that metal poor clusters may have a higher degree of orbital anisotropy than metal rich ones (Kruijssen 2015). Our models do not support this statement, suggesting that kinematic evidence of cluster accretion may become non-existent not long after a dwarf merger event. Minor mergers with galaxies that contain their own bi-modal GC population may also erase any relationship between orbital anisotropy and cluster type that was established when the central galaxy first formed. However, we also cannot rule out greater differences between the red and blue anisotropy profiles due to the clear degeneracy between R_β and $R_{f\alpha}$. We do find evidence in M87 that metal rich clusters are more under-filling than blue clusters at all R_{gc} , which indicates metal rich clusters either form more compact than metal poor clusters or expand at a slower rate.

Unfortunately, our best fit model to M87 still produces too many small clusters at low and high R_{gc} . Factors which may explain this difference between our model and observed cluster sizes include our choice for the functional form of the β profile in Equation 4, our assumption that $n(R_{gc})$ continues beyond the observational dataset and the possible existence of a third cluster sub-population with an intermediate metallicity between red and blue clusters found by Strader et al. (2011) and Agnello et al. (2014). With respect to the functional form of the β profile, allowing inner clusters to have preferentially tangential orbits and outer clusters to have a near isotropic distribution of orbits (the latter of which was found by Zhu et al. (2014)) would increase the mean r_h of clusters in the inner and outer regions

of M87. Additionally, in the Agnello et al. (2014) model of M87, the velocity dispersion for each sub-population changes as a function of R_{gc} which would also affect how the distribution of cluster orbits changes with R_{gc} . Future applications of our model will take into consideration the existence of more than two sub-populations, radially dependent velocity dispersions, different extrapolations of $n(R_{gc})$ and different functional forms of $\beta(r_{gc})$.

5.2 NGC 1399

The model which best reproduces the observed distribution of cluster sizes in NGC 1399 is also found when modelling the red and blue sub-populations separately. The best fit values of R_β and $R_{f\alpha}$ in NGC 1399 are quite similar to M87. The only difference between the two populations is the clusters in NGC 1399 appear to be a bit more under-filling than clusters in M87, which is consistent with the tidal field of NGC 1399 being weaker than M87. Unfortunately the degeneracy between the two parameters in each galaxy are such that we cannot conclude whether or not both galaxies have the *exact* same anisotropy and tidal filling profiles. It is interesting to note that our model of NGC 1399 predicts the same flattening in the r_h - R_{gc} profile at large distances that our M87 model did, but in the case of NGC 1399 the observational profile supports this trend. Hence the decrease in β inferred by Agnello et al. (2014) and Zhu et al. (2014) either doesn't occur in NGC 1399 and our functional form of $\beta(r_{gc})$ is correct or the cluster population has not been studied out to large enough R_{gc} .

The general case of orbits becoming more radial and clusters becoming more under-filling with r_{gc} is still prevalent in both M87 and NGC 1399. The fact that both galaxies are at the centre of large clusters is likely the common factor, as they formed via the hierarchical merging of smaller galaxies and neighbouring galaxies are continuously perturbing the outer cluster populations. Hence the outer regions of these galaxies cannot truly reach equilibrium. As we will see for NGC 5128 in the following section, a galaxy in isolation may in fact come closer to some sort of dynamical equilibrium.

5.3 NGC 5128

The mass profile and radial distribution of GCs in NGC 5128 is such that α is already quite low (0.46) if cluster orbits are all assumed circular. Allowing for an isotropic distribution of orbits, with the smaller velocity dispersion of NGC 5128, results in clusters having a higher mean eccentricity than either M87 or NGC 1399 and therefore a smaller mean size at a given r_{gc} . Furthermore, assuming an isotropic distribution of orbits, the radial distribution and velocity dispersion of GCs in NGC 5128 combine with its mass profile to yield a shallower increase in r_h with R_{gc} than either M87 or NGC 1399. Hence for NGC 5128, the distribution of cluster sizes is already well reproduced assuming the red and blue cluster populations are both primarily isotropic and tidally filling. For models where β and R_f are functions of r_{gc} , we see the degeneracy between R_β and $R_{f\alpha}$ in NGC 5128 is quite different from either M87 or NGC 1399. While differences between the galaxies can be attributed to them having different mass

profiles and GC radial distributions, the key issues are the lower velocity dispersion and small number of the observed GCs in NGC 5128 compared to M87 and NGC 1399.

The lower velocity dispersion and smaller number of the observed GCs in NGC 5128 result in there being almost no significant difference between the kinematic and structural properties of models with $\beta = 0$ and $R_f = 1$ and models with moderate to high values of R_β and $R_{f\alpha}$. And as discussed in Section 4.4, we were unable to constrain the degeneracy between R_β and $R_{f\alpha}$ based on kinematic studies of NGC 5128. Trying to model the red and blue cluster populations separately also did not improve the fit to the observations, indicating both sub-populations have the same kinematic properties. With Woodley et al. (2010b) suggesting that the kinematic properties of NGC 5128 indicate very little (if any) radial anisotropy is present in NGC 5128, any model with $\langle \beta \rangle \sim 0$ cannot be ruled out. Measuring GC sizes over a larger range in R_{gc} and a more detailed study of anisotropy in NGC 5128 are necessary in order to place stronger constraints on R_β and $R_{f\alpha}$ and minimize the uncertainty associated with best fit anisotropy and tidal filling profiles.

If NGC 5128 has a primarily isotropic population, it would suggest that NGC 5128 was assembled during an initial fast accretion phase (e.g. Biviano & Poggianti 2009) and has undergone few recent major mergers. Hence over 12 Gyr, any clusters accreted during this initial fast accretion will have their radial orbits decay and will have been pulled towards the centre of the galaxy (Goodman & Binney 1984; Lee & Goodman 1989; Cipolina & Bertin 1994). NGC 5128 is known to have several observational features (e.g. central black holes, jets, dust lanes) that are also seen in the majority of giant elliptical galaxies and are consistent with a history of mergers and on-going accretion events (van Dokkum 2003; Harris 2010; Rejkuba et al. 2011). However, since NGC 5128 is not a BCG like M87 and NGC 1399, it has likely not undergone as many mergers or accretion events. Furthermore, NGC 5128 does not have any massive galaxies or satellites nearby to perturb the outer cluster population.

6 CONCLUSIONS AND FUTURE WORK

We have successfully reproduced the distributions of GC sizes in three giant galaxies (M87, NGC 1399, and NGC 5128) by allowing cluster orbits to become more radial and clusters to become more under-filling with r_{gc} , in line with models and observations of galaxy structure and cluster populations (e.g. Côté et al. 2001; Prieto & Gnedin 2008; Zait, Hoffman, & Shlosman 2008; Weijmans et al. 2009; Gnedin & Prieto 2009; Ludlow et al. 2010; Strader et al. 2012; Kruijssen et al. 2012; Alexander & Gieles 2013; Puzia et al. 2014). For M87 and NGC 1399, both galaxies that are located at the centres of galaxy clusters, the global cluster populations have a high degree of radial anisotropy at larger r_{gc} and are primarily under-filling in the outer regions. Our findings are consistent with kinematic studies of each galaxy (e.g. Côté et al. 2001; Schuberth et al. 2010; Woodley et al. 2010b,c; Murphy, Gebhardt & Adams 2011; Agnello et al. 2014; Zhu et al. 2014), the assembly of giant galaxies via mergers and dwarf galaxy accretion (e.g. Schuberth et al. 2010; Kruijssen et al. 2012), and

the evolution of GC populations (Alexander & Gieles 2013; Webb et al. 2013a). NGC 5128 on the other hand was more difficult to model due to the lower number of observed clusters, but to first order appears to be nearly isotropic and tidally filling out to large R_{gc} .

The best fit orbital anisotropy and filling profiles of each of these galaxies come with significant uncertainty due to the strong degeneracy between R_β and $R_{f\alpha}$. Both parameters serve to decrease cluster size with r_{gc} . For M87 and NGC 1399, both datasets can be fitted by either a low R_β - high $R_{f\alpha}$ or low $R_{f\alpha}$ - high R_β model. However, kinematic studies of M87 and NGC 1399 allow us to rule out the low R_β - high $R_{f\alpha}$ cases, and we can accurately interpret M87 as having $R_\beta > 27$ kpc and $20 < R_{f\alpha} < 40$ kpc and NGC 1399 having $R_\beta > 13$ kpc and $10 < R_{f\alpha} < 30$ kpc. The best fit models are $R_\beta = 60$ kpc and $R_{f\alpha} = 34$ for M87 and $R_\beta = 76$ kpc and $R_{f\alpha} = 18$ for NGC 1399. Hence in both galaxies the orbits become moderately radial and clusters become tidally under-filling with r_{gc} . The fact that the acceptable range in $R_{f\alpha}$ is lower for NGC 1399 is consistent with the galaxy's mass profile increasing at a shallower rate, which suggests the present day relationship between r_h and R_{gc} is set upon cluster formation. Assuming clusters in both galaxies formed with the same initial distribution in r_h , only the innermost clusters and clusters with eccentric orbits will have expanded to the point of becoming tidally filling, with clusters in NGC 1399 becoming tidally under-filling at a lower R_{gc} than M87.

Unfortunately, since NGC 5128 is best fitted by models with $R_\beta > 5$ kpc and $R_{f\alpha} > 30$ kpc the degeneracy between the two parameters is much different than in M87 and NGC 1399. We attribute the larger uncertainty in R_β and $R_{f\alpha}$ to the lower velocity dispersion and fewer number of clusters in NGC 5128. So while kinematic studies of NGC 5128 suggest the population is primarily isotropic, we cannot confidently rule out models where β and R_f gradually change with R_{gc} .

Studying the models which best reproduce the distribution of red and blue cluster sizes in each galaxy individually, given the constraints implied by previous kinematic studies, also provides useful information regarding each galaxy. In both M87 and NGC 1399 we find that red clusters are significantly more under-filling than blue clusters at all R_{gc} , which suggests they formed more compact or expand at a slower rate. Furthermore, the best fit orbital anisotropy profiles of red and blue clusters in M87 and NGC 1399 are almost identical, suggesting the orbital anisotropy and tidally filling profiles of BCGs in general can be quite similar. If this is true, it would suggest that differences in the anisotropy profiles of accreted and non-accreted clusters will not exist if accretion took place a long time ago and the entire cluster population has had time to dynamically mix. Hence only the outermost clusters, which have yet to mix and are being perturbed by neighbouring satellites, will be found on radial orbits. Additional observations in each galaxy at large R_{gc} would be necessary to properly compare metal-poor and metal-rich clusters that may have just recently joined their central host.

For NGC 5128, modelling the red and blue GC populations separately actually results in a worse fit to observations than when the sub-populations are considered to have the same kinematic properties. This finding suggests the two sub-populations have had time to fully mix. Analysis of our models also suggests that NGC 5128 could be very differ-

ent from either M87 or NGC 1399, as we infer that NGC 5128 has a nearly isotropic and tidally filling population of GCs. This difference may suggest NGC 5128 formed via a fast accretion phase. A fast-accretion phase, combined with the fact that NGC 5128 is an isolated galaxy with no major satellites to perturb the outer cluster population, could result in an isotropic distribution of cluster orbits at all R_{gc} .

Detailed kinematic models of cluster sub-populations which take into consideration how velocity dispersion changes a function of r_{gc} are required in order for us to place stronger constraints on R_β . Measuring cluster sizes and velocities over a larger range in R_{gc} will also help minimize the degeneracy between R_β and $R_{f\alpha}$. In order to better constrain $R_{f\alpha}$, models of how cluster mass and structure evolves in the tidal fields of giant galaxies are needed, including clusters that have been accreted via mergers. Ultimately, what we can say with more certainty is that best fit models to M87 and NGC 1399 are telling us that BCGs can have different formation and merger histories but still have their present-day GC populations evolving in similar environments. The best model fits to NGC 5128 on the other hand indicate that more isolated giant galaxies are different then their brightest cluster galaxies counterparts. Hence differences between forming via an initial fast accretion stage followed by either slow or minor accretions/mergers versus having a longer dynamical history and neighbouring perturbing galaxies all leave different imprints on the cluster population in the form of its orbital anisotropy and tidal filling profiles.

7 ACKNOWLEDGEMENTS

We would like to thank the referee for constructive comments and suggestions regarding the presentation of the paper. JW, WEH and AS also acknowledge financial support through research grants and scholarships from the Natural Sciences and Engineering Research Council of Canada. M.P. acknowledges financial support from PRIN-INAF 2014 "Fornax Cluster Imaging and Spectroscopic Deep Survey".

REFERENCES

- Agnello, A., Evans, N.W., Romanowsky, A.J., Brodie, J.P. 2014, MNRAS, 442, 3299
- Alexander, P. E. R. & Gieles, M. 2013, MNRAS, 432L, 1
- Baumgardt H., Makino J. 2003, MNRAS, 340, 227
- Bertin, G. & Varri, A. L. 2008, ApJ, 689, 1005
- Bianchini, P., Renaud, F., Gieles, M., Varri, A.L. 2015, MNRAS, 447, 40
- Binney, J. & Tremaine, S. 2008, Galactic dynamics second edition (Princeton, NJ, Princeton University Press, 1987, 747 p.)
- Biviano, A. & Poggianti, B. M. 2009, A&A, 501, 419
- Blakeslee, J. P., J rdan, A., Mei, S., C t , P., Ferrarese, L., Infante, L., Peng, E.W., Tonry, J.L., West, M.J. 2009, ApJ, 694, 556
- Blom, C., Spitler, L. R., Forbes, D. 2012, MNRAS, 420, 37
- Brodie, J. P. & Strader, J. 2006, ARAA, 44, 193
- Casetti-Dinescu, D.I., Girard, T.M., Herrera, D., van Altena, W.E., L pez, C.E., Castillo, D.J. 2007, AJ, 134, 195

- Casetti-Dinescu, D.I., Girard, T.M., Jíková, L., van Altena, W.F., Podestá, F., López, C.E. 2013, *AJ*, 146, 33
- Cipolina, M. & Bertin, G. 1994, *AA*, 288, 43
- Côté, P., McLaughlin, D.E., Hanes, D.A., Bridges, T.J., Geisler, D., Merrid, D., Hesser, J.E., Harris, G.L.H., Lee, M.G., 2001, *ApJ*, 559, 828, 257B
- D'Abrusco, R., Fabbiano, G., Zezas, A. 2015, *ApJ*, 805, 26
- D'Abrusco, R., Fabbiano, G., Brassington, N.J. 2014a, *ApJ*, 783, 19
- D'Abrusco, R., Fabbiano, G., Mineo, S., Strader, J., Fragos, T., Kim, D.-W., Luo, B., Zezas, A. 2014b, *ApJ*, 783, 18
- D'Abrusco, R., Fabbiano, G., Strader, J., Zezas, A., Mineo, S., Fragos, T., Bonfini, P., Luo, B., Kim, D.-W., King A 2013, *ApJ*, 773, 87
- Deason, A.J., Belokurov, V., Evans, N.W., McCarthy, I.G. 2012, *ApJ*, 748, 2
- de Vaucouleurs, G., & Nieto, J.-L. 1978, *ApJ*, 220, 449
- Dehnen, W. 1993, *MNRAS*, 265, 250
- Dinescu, D.I., Girard, T.M., van Altena, W.E. 1999, *AJ*, 117, 1792
- Dunn, L.P. & Jerjen, H. 2006, *AJ*, 132, 1384
- Fall, S. M. & Zhang, Q., 2001, *ApJ*, 561, 751
- Gieles, M., Heggie, D. C., Zhao H. 2011, *MNRAS*, 413, 2509
- Gnedin, O. Y., & Prieto, J. L. 2009, in *ESO Astrophysics Symp.: Globular Clusters-Guides to Galaxies* (Berlin: Springer), 323
- Gómez, M. & Woodley, K.A. 2007, *ApJ*, 670, L105
- Goodman, J. & Binney, J.J. 1984, *MNRAS*, 207, 511
- Harris, W. E. 1996, *AJ*, 112, 1487, 2010 Edition
- Harris, W.E. 2009a, *ApJ*, 703, 939
- Harris, W.E. 2009b, *ApJ*, 699, 254
- Harris, W.E., Spitler, L.R., Forbes, D.A., Bailin, J. 2010, *MNRAS*, 401, 1965
- Harris, G.L.H., Rejkuba, M., Harris, W.E. 2010, *PASA*, 27, 457
- Harris, William E., Harris, G.L.H., Hudson M.J. 2015, *ApJ*, 806, 36
- Henon M. 1961, *Annales d'Astrophysique*, 24, 369
- Innanen, K. A., Harris, W.E., Webbink, R.F. 1983, *AJ*, 88, 338
- Jórdan, A. 2004, *ApJ*, 613, L117
- Jórdan, A., Côté, P., Blakeslee, J. P., Ferrarese, L., McLaughlin, D. E., Mei, S., Peng, E. W., Tonry, J. L., Merrit, D., Milosavljević, M., Sarazin, C. L., Sivakoff, G. R., West, M. J., 2005, *ApJ*, 634, 1002
- Kennedy, G.F. 2014, *MNRAS*, 444, 3328
- King, I. R. 1962, *AJ*, 67, 471
- Kormendy, J., Fisher, D.B., Cornell, M.E., Bender, R. 2009, *ApJS*, 182, 216
- Kravtsov, A.V. & Gnedin, O.Y. 2005, *ApJ*, 623, 650
- Kruijssen, J.M.D., Pelupessy, F.I., Lamers, H.J.G.L.M., Portegies Zwart, S.F., Bastian, N., Icke, V. 2012, *MNRAS*, 421, 1927
- Kruijssen, J.M.D. 2014, *Classical and Quantum Gravity*, 31, 244006
- Kruijssen, J.M.D. 2015, *MNRAS*, 454, 1658
- Kundu, A. & Whitmore, B. C. 1998, *AJ*, 116, 2841
- Kundu, A., Whitmore, B. C., Sparks, W. B., Macchetto, F. D., Zepf, S. E., Ashman, K. M. 1999, *ApJ*, 513, 733
- Küpper, A. H. W., Kroupa, P., Baumgardt, H., Heggie, D. C. 2010, *MNRAS*, 407, 2260
- Larsen, S. S. 1999, *Å*, 139, 393
- Larsen, S. S., Brodie, J. P., Huchra, J. P., Forbes, D. A., Grillmair, C. J. 2001, *AJ*, 121, 2974
- Lee, M.H. & Goodman, J. 1989, *ApJ*, 343, 594
- Li, H. & Gnedin, O.Y. 2014, *ApJ*, 796, 10
- Longobardi, A., Arnaboldi, M., Gerhard, O., Mihos, J. C. 2015, *A&A*, 579, 135
- Ludlow, A. D., Navarro, J. F., Springler, V., Vogelsberger, M., Wang, J., White, S. D. M., Jenkins, A., & Frenk, C. S. 2010, *MNRAS*, 406, 137
- Madrid, J.P., Hurley, J.R., Martig, M., 2014, *ApJ*, 784, 95
- McLaughlin, D. E. & van der Marel, R. P. 2005, *ApJs*, 161, 304
- McLaughlin, D. E. 1999, *ApJ*, 512, L9
- Miholics, M., Webb, J., Sills, A., 2014, *MNRAS*, 445, 2872
- Miholics, M., Webb, J., Sills, A., 2016, *MNRAS*, 456, 240
- Moreno, E., Pichardo, B., Velázquez, H. 2014, *ApJ*, 793, 110
- Murphy, J.D., Gebhardt, K. & Adams, J.J. 2011, *ApJ*, 729, 129
- Navarro, J. F., Frenk, C. S., & White, S. D. M. 1997, *ApJ*, 490, 493
- Paolillo, M., Fabbiano, G., Peres, G. Kim, D.-W. 2002, *ApJ*, 565, 883
- Paolillo, M., Puzia, T. H., Goudfrooij, P., Zepf, S. E., Maccarone, T. J., Kundu, A., Fabbiano, G., Angelini, L. 2011, *ApJ*, 736, 90
- Peng, E. W., Ford, H. C., & Freeman, K. C. 2004, *ApJ*, 602, 685
- Peng, E. W., Ford, H. C., & Freeman, K. C. 2004, *ApJ*, 602, 705
- Peng, E.W., Jórdan, A., Côté, P., Blakeslee, S., Ferrarese, L., Mei, S., West, M. J., Merritt, D., Milosavljević, M., Tonry, J. L. 2006, *ApJ*, 639, 95
- Peng, E.W., Ho, L. C., Impey, C. D., & Rix, H.-W. 2010, *AJ*, 139, 2097
- Pierce, M. J., Welch, D. L., McClure, R. D., van den Bergh, S., Racine, R., & Stetson, P. B. 1994, *Nature*, 371, 385
- Prieto, J. L. & Gnedin, O. Y. 2008, *ApJ*, 689, 919
- Puzia, T.H., Paolillo, M., Goudfrooij, P., Maccarone, T.J., Fabbiano, G., Angelini, L. 2014, *ApJ*, 786, 78
- Rejkuba, M., Harris, W.E., Greggio, L., Harris, G.L.H. 2011, *A&A*, 526, 123
- Renaud, F., Gieles, M., Christian, M. 2011, *MNRAS*, 418, 759
- Renaud, F. & Gieles, M. 2015, *MNRAS*, 448, 341
- Romanowsky, A.J. & Kochanek, C.S. 2001, *ApJ*, 553, 722
- Romanowsky, A.J., Strader, J., Brodie, J.P., Mihos, J.C., Spitler, L.R., Forbes, D.A., Foster, C., Arnold, J.A. 2012, *ApJ*, 748, 29
- Sippel, A.C., Hurley, J.R., Madrid, J.P., Harris, W.E. 2012, *MNRAS*, 427, 167
- Schiminovich, D., van Gorkum, J. H., van der Hulst, J. M., & Kasow, S. 1994, *ApJ*, 423, L101
- Schuberth, Y., Richtler, T., Hilker, M., Dirsch, B., Bassin, L.P., Romanowsky, A.J., Infante, L. 2010, *A&A*, 512, 52
- Schulman, R. D., Glebbeek, E., Sills, A. 2012, *MNRAS*, 420, 651
- Spitler, L.R., Larsen, S.S., Strader, J., Brodie, J.P., Forbes, D.A., Beasley, M.A. 2006, *AJ*, 132, 1593
- Strader, J., Romanowsky, A.J., Brodie, J.P., Spitler, L.R., Beasley, M.A., Arnold, J.A., Tamura, N., Sharples, R.M.,

- Arimoto, N. 2011, *APJS*, 197, 33
- Strader, J., Fabbiano, G., Luo, B., Kim, D., Brodie, J.P., Fragos, T., Gallagher, J.S., Kalogera, V., King, A., Zezas, A. 2012, *ApJ*, 760, 87
- Tal, T., van Dokkum, P. G., Nelan, J., Bezanson, R. 2009, *AJ*, 138, 1417
- Tonini, C. 2013, *ApJ*, 762, 39
- Tonry, J. L., Dressler, A., Blakeslee, J. P., Ajhar, E.A., Fletcher, A.B., Luppino, G.A., Metzger, M.R., Moore, C.B. 2001, *ApJ*, 546, 681
- Tremaine, S., Richstone, D.O., Byun, Y.-L., Dressler, A., Faber, S. M., Grillmair, C., Kormendy, J. and Lauer, T. R. 1994, *AJ*, 107, 634
- Usher, C., Forbes, D.A., Spitler, L.R., Brodie, J.P., Romanowsky, A.J., Strader, J., Woodley, K.A. 2013, *MNRAS*, 436, 1172
- van den Bergh, S. 2003, *ApJ*, 590, 797
- van Dokkum, P. G. 2005, *AJ*, 130, 2647
- Vesperini, E., Zepf, S. E., Kundu, A., Ashman, K. M. 2003, *ApJ*, 593, 760
- von Hoerner, S. 1957, *ApJ*, 125, 451
- Webb, J.J, Sills, A., Harris, W.E. 2012, *ApJ*, 746, 93
- Webb, J.J., Harris, W.E., Sills, A., Hurley, J.R. 2013a, *ApJ*, 764, 124
- Webb, J.J, Sills, A., Harris, W.E. 2013b, *ApJ*, 779, 94
- Webb, J.J., Sills, A., Harris, W.E., Hurley, J.R. 2014, *MNRAS*, 445, 1048
- Weijmans, A., Cappellari, M., Bacon, R., de Zeeuw, P. T., Emsellem, E., Falcon-Barroso, J., Kuntschner, H., McDermid, R. M., van den Bosch, R. C. E., and van de Ven, G., 2009, *MNRAS*, 398, 561
- Woodley, K.A., Harris, W.E., Beasley, M.A., Peng, E.W., Bridges, T.J., Forbes, D.A., Harris, G.L.H. 2007, *AJ*, 134, 494
- Woodley, K.A. & Gómez, M. 2010a, *PASA*, 27, 379
- Woodley, K.A., Gómez, M., Harris, W.E., Geisler, D., Harris, G.L.H. 2010b, *AJ*, 139, 1871
- Woodley, K.A., Harris, W.E., Puzia, T.H., Gómez, M., Harris, G.L.H., Geisler, D. 2010c, *ApJ*, 708, 1335
- Woodley, K. 2012, *AAS Meeting #220, #438.07*
- Wu, X., Gerhard, O., Naab, T., Oser, L., Martinez-Valpuesta, I., Hilz, M., Churazov, E., Lyskova, N. 2014, *MNRAS*, 438, 2701
- Zait, A., Hoffman, Y. & Shlosman, I. 2008, *ApJ*, 682, 835
- Zepf, S. E. & Ashman, K. M. 1993, *MNRAS*, 264, 611
- Zhu, L., Long, R.J., Mao, S., Peng, E.W., Liu, C., Caldwell, N., Li, B., Blakeslee, J.P., Côté, P., Cuillandre, J.C., Durrell, P., Emsellem E., Ferrarese, L., Gwyn, S., Jórdan, A., Lançon, A., Mei, S., Muñoz, R., Puzia, T. 2014, *ApJ*, 729, 59